Benchmarking iSALE and CTH shock physics codes to in situ high-velocity impact experiments into Fe-Ni targets

A. M. Alexander[1,2], S. Marchi[1], S. Chocron[3], and J. Walker[3]

[1]Southwest Research Institute, Boulder, CO 80302, USA.

[2]University of Colorado Boulder, Boulder, CO, 80309, USA.

[3]Southwest Research Institute, San Antonio, TX 78238, USA.

Corresponding author: Amanda M. Alexander (alexander@boulder.swri.edu)

Key Points:

- We conducted several small-scale 2D numerical shock physics simulations in iSALE and CTH into Fe-Ni targets.
- We measured material strength parameters from mechanical tests at low and high strain-rates and relevant temperatures for Fe-Ni materials.
- The simulated craters are within 5% for Fe-Ni manufactured targets and 15% for Gibeon meteorite cubes as compared to the experimental sizes.

Abstract

Cratering is a prominent evolutionary process on asteroids. Crater morphologies, regolith generation, bulk fracturing and projectile implantation are all examples of asteroidal surface evolution resulting from impact processes. With the upcoming launch of the *Psyche* mission in 2022, followed by the spacecraft's arrival at the 225-km presumed metal-rich asteroid, characterizing impact processes on relevant metal bodies is key for interpreting mission data. Small-scale impact experiments into metals (e.g., iron, aluminum, copper, steel) have shown that crater morphologies into these materials are different than rocky targets — exhibiting notable distinctive features such as raised, sharp rims, and deeper cavities. While several impact codes have been used to simulate and benchmark laboratory scale impacts on rocky targets, it has not yet been shown how well these codes match observed crater shapes in Fe-Ni materials which may constitute the metallic component of Psyche. Here we have used iSALE and CTH shock physics codes to simulate and compare with the observed experimental crater morphologies in Fe-Ni targets. It was found that, when using material strength parameters directly measured in laboratory mechanical tests, at low and high strain-rates and relevant temperatures, it is possible to closely match crater diameters and depths from the impact tests.

Plain Language Summary

The NASA mission to Asteroid (16) Psyche will launch in 2022. While impact craters are readily observed on rocky and icy bodies throughout the solar system, craters on surfaces made of metal are not as well understood. To best understand and interpret data and observations from the spacecraft at Psyche, cratering experiments have been conducted into centimeter-sized iron-nickel cylinders

and iron meteorite cubes. In this work, we use numerical modeling to reproduce cratering experiments at the millimeter and centimeter scale to ensure shock physics software like iSALE and CTH can be used to explore cratering at the larger scale (meters to kilometers) on metal-rich surfaces like the asteroid Psyche.

1 Introduction

The NASA *Psyche* mission is scheduled to launch in 2022. The 225-km asteroid Psyche was chosen as the mission target because remote sensing data (radar, density, etc.) indicated a likely metallic composition (e.g., Konopoliv et al., 2011; Matter et al., 2013; Shepard et al., 2015). Previous missions have visited rocky asteroids at close range (e.g., *Galileo*, *Dawn*, *Rosetta*) revealing that cratering is the primary evolutionary process of main belt asteroid surfaces. As such, the selection of the *Psyche* mission triggered an increased interest in the scientific community to better understand cratering into metallic materials relevant to asteroids (e.g., Marchi et al., 2020; Libourel et al., 2019; Raducan et al., 2020; Ogawa et al., 2021). These impact experiments have provided preliminary insight as to crater dimensions, depth, and overall morphology for iron meteorites and their lab made proxy Fe-Ni alloys, showing that cratering into Fe-Ni targets is remarkably different from rocky targets. Additional metallic targets, such as aluminum and copper, have been investigated (e.g., Horz et al., 1995; Burchell and Mackay, 1998, Hernandez et al., 2006; Daly and Schultz, 2018), but in light of these non-asteroidal compositions, their applicability to Psyche requires further consideration.

The selection of the *Psyche* mission also prompted continued telescopic observations. These observations, coupled with revised mass and shape modeling estimates, indicate that Psyche may contain less metal than previously thought. The current best interpretation of available data to date suggests that Psyche may have 30-60 vol.% metal (Elkins-Tanton et al., 2020). This conclusion primarily rests on revised mass (lower) and volume (larger) estimates combined with radar, spectral and thermal inertia observations. Psyche may be dominantly metallic (Fe-Ni alloys), but may contain up to 60% porosity (Elkins-Tanton et al., 2020) are notions used to explain the current best estimate of Psyche' density (4.1-4.2 g/cm3, Ferrais et al., 2020). Alternatively, Psyche could be an assemblage made dominantly of Fe-Ni with up to 5-10 wt.% low-Fe silicates and 8-17 wt.% and ~35% porosity (Cantillo et al., 2021, Elkins-Tanton et al., 2020, Sanchez et al., 2017, Takir et al., 2017). The origin of extensive porosity on Psyche is not understood. A possibility is that porosity could be due to impact-generated fracturing perhaps as the result of one or more hit-and-run collisions with subsequent re-accumulation, and/or the result of billions of years of collisional evolution in the main belt. Interestingly, the hypothesis that Psyche may be heavily fractured is bolstered by our recent impact experiments on Fe-Ni targets (Marchi et al., 2020), in which impacts cause metal cracking thereby introducing significant bulk porosity. The applicability of these lab-scale experiments to Psyche, however, remains to be investigated.

Regardless of the specific nature of Psyche composition, impact processes are important for the evolution of the surface and have strong influences on overall bulk porosity, regolith generation and projectile implantation onto a metallic object. To investigate how impacts alter the surface of metal-rich bodies, like Psyche, we compare small-scale *in situ* high-velocity experiments (Marchi et al., 2020) to simulated crater morphologies. In this work, we benchmark iSALE and CTH shock physics codes in 2D against our *in situ* high-velocity impacts on Fe-Ni targets. We compare results from iSALE and CTH and evaluate strengths and limitations of both codes for specific planetary applications, such as large-scale collisions on asteroid Psyche.

2 Methods

We simulated all 18 of the vertical (90 degrees, overhead) impacts from Marchi et al. (2020) (Table 1) into the Fe-Ni ingots and iron meteorite Gibeon targets using the iSALE-2D shock physics code and two (#2.06 and #2.11 from Table 1) using the CTH shock physics suite. iSALE is an extension of the SALE hydrocode (Amsden et al., 1980). To simulate hypervelocity impact processes in solid materials SALE was modified to include an elasto-plastic constitutive model, fragmentation models, various equations of state (EoS), and multiple materials (Melosh et al., 1992; Ivanov et al., 1997). More recent improvements include a modified strength model (Collins et al., 2004), a porosity compaction model (Wünnemann et al., 2006; Collins et al., 2011) and a dilatancy model (Collins, 2014). CTH is an Eulerian shock-physics code developed at Sandia National Laboratories (McGlaun et al., 1990) and has been used for a variety of high-velocity deformation problems (including planetary cratering). CTH has models for multi-phase, elastic, viscoplastic, porous, and energetic materials. Three-dimensional rectangular meshes, two-dimensional rectangular and cylindrical meshes, as well as one-dimensional rectilinear, cylindrical, and spherical meshes are available. CTH can utilize adaptive mesh refinement and uses second-order accurate numerical methods that reduce dispersion and dissipation to produce accurate and efficient results.

AVGR #		Impactor material	Impactor size	Velocity (km/s)	Target Temp. (K)
	I-90 (a)	Al	S3		
	I-90 (a)	Al	S3		
	I-94 (b)	Qz	S3		
	I-94 (b)	Qz	S3		
	I-94 (b)	Qz	S1		
	I-94 (b)	Qz	S1		
	I-90 (b)	Qz	S3		
	I-90 (b)	Qz	S3		
	I-94 (b)	Qz	S3		
	I-94 (b)	Qz	S3		
	I-94 (b)	Qz	S1		
	I-94 (b)	Qz	S1		

I-90 (b)	Qz	S3
G	Qz	S1
G	Qz	S1
G	Qz	S1
G	Qz	S1
G	Qz	S3

Table 1. Summary of simulations performed to match all vertical (90 degrees/head-on) experiments from Marchi et al. (2020). Note that impactor sizes are presented as S1: 3.175 mm and S3: 6.35 mm diameter, respectively. Only experiments #2.06 and #2.11 were simulated in CTH as well as iSALE. (a) and (b) indicate two batches of ingots.

2.1 Strength model and newly-measured parameters

We performed tensile tests on each of the three manufactured Fe-Ni ingots. The Johnson and Cook (JC) strength model is defined as (Johnson and Cook, 1983),

$$Y = (A + B\epsilon^N)(1 + C \ln \dot{\epsilon})[1 - (\frac{T - T_{\rm ref}}{T_m - T_{\rm ref}})^M] \qquad \text{Equ. 1}$$

where Y is yield strength, T is temperature, is the equivalent plastic strain, $\dot{\epsilon}$ is the strain rate (set to be 1 at the reference state in iSALE), A is the yield strength at the reference state, B, C, M and N are material constants, T_m is the melt temperature and $T_{\rm ref}$ is the reference temperature. We stress that the implementation of the JC strength model, as implemented in iSALE, neglects a temperature dependence for cases where the reference temperature of the material is greater than the surface temperature of the target. This effectively reduces the above equation to the following:

$$Y = (A + B\epsilon^N)(1 + C \ln \dot{\epsilon}) \qquad \text{Equ. 2}$$

To produce simulations where cooled target temperature dependence is properly accounted for within the strength model, we measured and implemented JC strength constants at 77 K (that is, lower than the cooled target temperatures). We performed tensile tests on the three ingots, I-90 (a), I-90 (b) and I-94 (b) at 77 K to determine the thermal constant, M. The other constants (A, B, C and N) were determined by compression tests. The Poisson ratio, elastic modulus and strength of each ingot were also measured. We derived the necessary parameters for aluminum (Al 6061-T6) by scaling the known parameters from room temperature to 77 K using the cryogenic data of Al6061-T6 from the Cryogenic Materials Data Handbook. Results of the strength tests are shown in Figure 1. Finally, we determined the input parameters for the Gibeon targets from strength versus temperature data in Gordon et al. (1970) to fit the thermal constant, M. We used the same strain-rate constant as the ingot I-94 (b) as it matches well with data from Gordon et al. (1970). We find that the Gibeon meteorite material is extremely ductile with an equivalent strain to failure of 180%. Table 3 outlines in detail the constants.

Description	Symbol	I-90 (a)	I-90 (b)	I-94 (b)	Gibeon	Alum.
Strain coef. A (MPa)	A	397	605	435	547	375
Strain coef. B (MPa)	B	861	793	574	340	114
Strain exponent	n	0.32	0.38	0.41	0.8	0.42
Strain constant	C	0.017	0.017	0.025	0.017	0.002
Thermal softening	m	0.72	0.70	0.70	0.55	1.70
Reference temperature (K)	T_{ref}	77	77	77	77	77

Table 2. The JC strength and thermal model parameters used in our iSALE simulations. These values were derived from compressional and tensile tests performed at 77 K and above in order for iSALE to include thermal softening on all targets, cooled and room temperature, as described in the text.

2.2 iSALE simulation set-up

Davison et al (2011) show that simulations at this scale can be approximated well with resolutions of 12-20 cells per projectile radius (CPPR), with little increase in accuracy beyond 20 CPPR for crater depth. As such, our simulations employ an Eulerian grid with square 1.5785×10^{-4} m cells, corresponding to resolutions of 20 CPPR. The high-resolution zone (HRZ) of this mesh consists of 220 x 360 cells. Beyond the HRZ, cell-size increases by a constant fraction of 1.05. As these are 2D simulations, we use cylindrical symmetry to approximate vertical impacts along the axis of symmetry (the y-axis). The right and left sides of the mesh have free-slip boundary conditions. The bottom and top have no-slip and outflow boundary conditions, respectively. Projectiles were simulated as 3.175 mm (aluminum and quartz) and 6.35 mm (quartz only) spheres with impact velocities that correspond to those reported from the experiments by Marchi et al. (2020).

For small-scale simulations such as these, the time when the transient crater is formed (when there is the maximum volume) is generally the same time as when the crater has finished forming (change in depth and diameter is minimized). Further, observations from the in situ experiments from Marchi et al (2020) show that the modification stage for impacts into these metallic materials is virtually non-existent, resulting in crater rims that appear frozen in place. For the materials in this work, the timeframe in which the transient crater is formed (and therefore, where we are approximating the end of the crater formation) seems to occur after 30-80 microseconds. For continuity, we take the longer end-member of 80 microseconds as the final crater stage to compare the results of all simulated craters with the experimental results. We ran simulations through 150 microseconds.

We simulated impacts into four different target materials with two different impactor materials based on laboratory measurements of the targets used in Marchi et al (2020). Table 3 lists the full details of the properties for each material. The quartz projectiles were approximated by using the ANEOS equation of

state for granite (Ivanov, 2000 and Pierazzo et al., 1997) and a thermal softening model after Ohnaka et al. (1995). Strength in the quartz projectiles is approximated by the "ROCK" strength model (Collins, 2004)—a pressure-dependent strength model which reduces shear strength with the accumulation of damage. The aluminum projectiles were approximated using the Tillotson equation of state for aluminum (Tillotson, 1962) and the JC strength and thermal softening (Johnson and Cook, 1983) models.

The experiments performed by Marchi et al. (2020) simulated in this work were on three distinct manufactured types, henceforth referred to as I-90 (a), I-90 (b), and I-94 (b) where each refers to Ingot (I), the compositional make-up (90 or 94 % Fe, and 10 or 6 % Ni, respectively), and which batch of experiments (a - hypervelocity experiments which took place in 2016 versus b- hypervelocity experiments that took place in 2019). We also simulated the five vertical impacts into the Gibeon meteorite targets. All target materials were simulated using the ANEOS equation of state for iron (Ivanov, 2000) and the JC strength and thermal softening (Johnson and Cook, 1983) models. For each distinct target material, we determined the necessary JC strength model parameters (see Table 2) from mechanical characterization tests performed in the laboratory. Finally, we define the surface temperature of the target in the simulation to match that of the temperature of the target from the in situ impact experiments (as temperature was noted to have a distinct effect on the material strength, discussed further in the next section).

Description	Symbol	aluminum	quartz	iron*
Equation of state		Tillo[a]	Aneos[b,c]	Aneos[d]
Strength model		JNCK[d]	ROCK[e]	JNCK
Thermal soft.		JNCK	OHNAKA[f]	JNCK
Poisson ratio		0.33	0.25	0.30
Density (kg/m^3)		2700	2620	7841
Specific heat capacity (J/kg/K)	C_p	8.96E+2	1.196E+3	4.509E+2
Melt temp. (K)	T_m	933	1500	1750

*Table 3. Description of iSALE simulation settings including the specific strength and thermal softening models used for each material. We elaborate on the particular parameters of the JNCK model in Table 2. *Iron parameters are those which we have derived experimentally. [a]Tillotson (1962); [b]Ivanov (2000a); [c]Pierazzo et al. (1997); [d]Johnson and Cook (1983); [e]Collins (2004); [f]Ohnaka (1995).*

2.3 CTH simulation set-up

We use version 11.1 of CTH and cylindrical symmetry for computations of 6.35 mm diameter quartz sphere impacting an iron ingot plate at 3.41 km/s (119 K) and 5.31 km/s (290 K), respectively (corresponding to the two in situ experiments numbered 2.06 and 2.11 in Marchi et al., 2020). Both ingots in the

experiments and simulations were of the type I-90 (b). We utilize the equations of state for quartz and iron, which are included in the CTH library. Since the strength of the impactor does not play a pivotal role in crater size, strength for the impactors is approximated to behave like Al-2024 from the CTH library (as there is no strength model within the CTH suite for quartz at this time). We implement the JC strength model within CTH for the iron ingot target material using the same input parameters described before (Table 2). The resolution (cell size) of these simulations is 0.03 cm.

3 Results

The measured crater diameters and depths for all of our iSALE/CTH simulations are shown in Table 4. We consider the spatial resolution (cell size) the error for the simulations and propagate to include error from the measurements (i.e., digital caliper and height gauge precision) when computing the relative crater depths and diameters between simulations and experiments (Figures 4 and 5). Both the simulated and experimental crater dimensions are measured from the pre-impact surface (y=0). In one case, in simulation #2.04, which is of the smallest size impactor at very low target temperature and very high velocity (end member scenarios for all three variables) that became unstable, producing dramatic numerical artifacts. To address this problem, we performed simulations for experiment # 2.04 at +1 K, +5 K and with a finer resolution. The values reported in this work are from the simulation at 119 K (+1 K).

Our simulations reproduce the crater dimensions reported in Marchi et al. (2020) on average within ~15% of the experimental values, with better precision when using laboratory-derived JC parameters for the Fe-Ni ingots (Figure 4). Notably, our iSALE simulations reproduce the crater diameters measured from our experiments into ingot targets on average with ~98.2% accuracy (denoted by the circular markers in Figure 4). Crater diameters into Gibeon targets are on average 9.2 ± 2.7% larger than the experiments. Crater depths are reproduced with iSALE within 3.5 ± 1.5% of the experimental values for ingots and within 11.6 ± 3.5% for Gibeon targets.

Both #2.06 and #2.11 impact experiments were into material I-90 (b), with the latter target being at room temperature and the former cooled. When comparing CTH output to iSALE, the crater depth for #2.06 is ~3.8 mm in CTH versus ~3.65 mm in iSALE and for #2.11 is ~5.9 mm versus ~6.35 mm in SALE. The CTH-produced crater diameters are larger (13.0 and 15.8 mm for #2.06 and #2.11) than in iSALE, and both are larger than the experiments. Given the coarser resolution in our CTH simulations, there is a bit more error in the CTH simulations than the iSALE simulations. Both iSALE and CTH show similar trends that cooled targets tend to overestimate crater diameters and depths more than room-temperature targets.

Exp. #	Target Type	T (K)	Exp. Depth (mm)	Sim. Depth (mm)	Sim/Exp Depth	Exp. Diam.
1.07	I90 (a)	297	7.0 ± 0.04	7.144	1.02	17.5 ± 0.03
1.14	I90 (a)	117	6.3 ± 0.04	6.826	1.08	16.9 ± 0.03

2.01	I94 (b)	133	3.8 ± 0.07	4.128	1.09	12.3 ± 0.04
2.02	I94 (b)	112	5.9 ± 0.04	5.855	0.99	14.7 ± 0.04
2.03	I94 (b)	123	1.8 ± 0.15	1.900	1.06	5.9 ± 0.09
2.04	I94 (b)	118	3.0 ± 0.09	3.254	1.08	7.8 ± 0.07
2.05	I90 (b)	120	5.6 ± 0.05	6.349	1.13	15.7 ± 0.03
2.06	I90 (b)	119	3.3 ± 0.08	3.650	1.11	11.6 ± 0.04
2.07	I94 (b)	293	7.1 ± 0.04	7.620	1.07	18.2 ± 0.03
2.08	I94 (b)	293	4.2 ± 0.04	3.652	0.87	13.1 ± 0.04
2.09	I94 (b)	289	3.2 ± 0.07	3.016	0.94	8.2 ± 0.06
2.10	I94 (b)	289	1.7 ± 0.13	1.560	0.92	5.5 ± 0.09
2.11	I90 (b)	290	6.1 ± 0.04	6.350	1.04	15.6 ± 0.03
2.14	G	296	2.5 ± 0.12	2.937	1.17	6.9 ± 0.08
2.15	G	109	1.8 ± 0.16	2.064	1.15	5.3 ± 0.11
2.16	G	116	3.0 ± 0.10	3.651	1.22	6.9 ± 0.09
3.01	G	292	3.2 ± 0.08	3.109	0.97	8.9 ± 0.05
3.08	G	122	6.0 ± 0.05	6.826	1.14	14.5 ± 0.04
2.06 CTH	I90 (b)	119	3.3 ± 0.08	3.8	1.14	11.6 ± 0.04
2.11 CTH	I90 (b)	290	6.1 ± 0.04	5.9	0.97	15.6 ± 0.03

Table 4. Detailed list of simulation results for crater depth and diameter as compared to the measurements from Marchi et al (2020). The experimental measurements include measurement diameter, depth, and caliper precision to 0.25, 0.5, and 0.01 mm, respectively. Simulated crater depths and diameters are rounded to the nearest cell-size resolution, which is ~0.15 mm in iSALE and ~0.03 cm in CTH.

4 Discussion

This work made use of experimentally-determined and derived JC strength model parameters. Similar studies into Fe-Ni and Psyche-analogous materials have used JC input parameters for Armco Iron (e.g., Raducan et al., 2020 and Ogawa et al., 2021). Given that Marchi et al. (2020) reported that target temperature has measurable effects on strength, where cooled targets are up to 20% stronger than room temperature targets, we emphasize that measuring the strength and finding the JC parameters at a cold temperature (77 K) is necessary to include the temperature dependence portion of the JC strength model in cases where the target reference temperature is greater than the target surface temperature. Figure 5 illustrates the distinct effect temperature has on the strength of a material in the JC strength model.

Unlike silicates, which are brittle under compression, metals typically undergo ductile deformation, meaning they permanently deform by bending or flowing without becoming weaker, breaking, or failing. Analysis of our tensile tests has shown an equivalent plastic strain to failure,ϵ_f,of up to 1.8 (or 180%) for Fe-Ni ingots as well as the Gibeon meteorite. Yet, extensive cracking and fracturing — indicative of brittle deformation — were observed in some of the targets in the

impact experiments. There is no current damage model for metals in iSALE, a major limitation in modeling the observed cracking. Although CTH is less widely used in the planetary science community, it proves to be a valid and useful tool in simulating impacts into metal. The CTH suite includes both a Johnson and Cook strength model (Johnson and Cook, 1983) and a Johnson and Cook fracture model (Johnson and Cook, 1985), which we plan to explore the implementation of in the JC fracture model into iSALE in future work.

5 Conclusion

In this work, we demonstrate that the iSALE and CTH shock-physics codes are an applicable tool to model impacts into Fe-Ni objects for what concerns crater morphology. To improve our understanding of cratering in Fe-Ni alloy compositions that overlap that of iron meteorites (a possible major component of Psyche), we have performed 18 iSALE and 2 CTH simulations based on the set-up of hypervelocity impact experiments performed at the NASA AMES Vertical Gun Range in Marchi et al (2020). Observation and analysis show that the strength of Fe-Ni and iron meteorite targets is dependent on target temperature. Moreover, crater morphologies of these materials are characterized by sharp, raised rims and deep cavities — these observations are in agreement with the output of our numerical simulations. We find that both iSALE and CTH reproduce crater sizes and depth to within 15% for Fe-Ni materials and are adequate tools for studying crater morphology in Fe-Ni targets. These tools provide a good base for simulating large-scale collisions on Psyche, provided the relevant material parameters (including temperature and dependence) are used.

6 References

1. A.A. Amsden, H.M. Ruppel, C.W. Hirt, Sale: A Simplified ALE Computer Program For Fluid Flow At All Speeds, Los Alamos Scientific Lab., Nm (Usa), 1980. Https://Doi.Org/10.2172/5176006.
2. M.J. Burchell, N.G. Mackay, Crater Ellipticity In Hypervelocity Impacts On Metals, J. Geophys. Res. 103 (1998) 22761–22774. Https://Doi.Org/10.1029/98je02143.
3. G.S. Collins, H.J. Melosh, K. Wünnemann, Improvements To The - Porous Compaction Model For Simulating Impacts Into High-porosity Solar System Objects, International Journal Of Impact Engineering. 38 (2011) 434–439. Https://Doi.Org/10.1016/J.Ijimpeng.2010.10.013.
4. G.S. Collins, H.J. Melosh, B.A. Ivanov, Modeling Damage And Deformation In Impact Simulations, Meteoritics & Planetary Science. 39 (2004) 217–231. Https://Doi.Org/10.1111/J.1945-5100.2004.Tb00337.X.
5. Daly, R.T., & Schultz, P.H., Projectile Preservation During Oblique Hypervelocity Impacts, Meteoritics & Planetary Science. 53 (2018) 1364–1390. Https://Doi.Org/Doi: 10.1111/Maps.13081.
6. T.M. Davison, G.S. Collins, D. Elbeshausen, K. Wünnemann, A.

Kearsley, Numerical Modeling Of Oblique Hypervelocity Impacts On Strong Ductile Targets: Oblique Hypervelocity Impacts On Ductile Targets, Meteoritics & Planetary Science. 46 (2011) 1510–1524. Https://Doi.Org/10.1111/J.1945-5100.2011.01246.X.

7. L.T. Elkins-tanton, E. Asphaug, J.F.B. Iii, H. Bercovici, B. Bills, R. Binzel, W.F. Bottke, S. Dibb, D.J. Lawrence, S. Marchi, T.J. Mccoy, R. Oran, R.S. Park, P.N. Peplowski, T.H. Prettyman, C.T. Russell, L. Schaefer, B.P. Weiss, M.A. Wieczorek, M.T. Zuber, Composition And Formation Of (16) Psyche, (N.D.) 41.

8. M. Ferrais, P. Vernazza, L. Jorda, N. Rambaux, J. Hanuš, B. Carry, F. Marchis, M. Marsset, M. Viikinkoski, M. Brož, R. Fetick, A. Drouard, T. Fusco, M. Birlan, E. Podlewska-gaca, E. Jehin, P. Bartczak, J. Berthier, J. Castillo-rogez, F. Cipriani, F. Colas, G. Dudziński, C. Dumas, J. Ďurech, M. Kaasalainen, A. Kryszczynska, P. Lamy, H. Le Coroller, A. Marciniak, T. Michalowski, P. Michel, T. Santana-ros, P. Tanga, F. Vachier, A. Vigan, O. Witasse, B. Yang, Asteroid (16) Psyche's Primordial Shape: A Possible Jacobi Ellipsoid, A&A. 638 (2020) L15. Https://Doi.Org/10.1051/0004-6361/202038100.

9. R.B. Gordon, Mechanical Properties Of Iron Meteorites And The Structure Of Their Parent Planets, J. Geophys. Res. 75 (1970) 439–447. Https://Doi.Org/10.1029/Jb075i002p00439.

10. Hernandez, V. S., Murr, L. E.. & Anchondo I. A., Experimental Observations And Computer Simulations For Metallic Projectile Fragmentation And Impact Crater Development In Thick Metal Targets, International Journal Of Impact Engineering . 32 (2006) 1981-1999.

11. F. Horz, M.J. Cintala, R.P. Bernhard, F. Cardenas, W.E. Davidson, G. Haynes, T.H. See, J.L. Winkler, Penetration Experiments In Aluminum 1100 Targets Using Soda-lime Glass Projectiles, Nasa Sti/Recon Technical Report N. 96 (1995). Http://Adsabs.Harvard.Edu/Abs/1995stin...9615990h (Accessed May 20, 2021).

12. G. R. Johnson and W. H. Cook, "A Constitutive Model and Data for Metals Subjected to Large Strains, High Strain Rates and High Temperatures," Proceedings of the Seventh International Symposium on Ballistics, The Hague, The Netherlands, April 1983

13. A.S. Konopliv, S.W. Asmar, W.M. Folkner, Ö. Karatekin, D.C. Nunes, S.E. Smrekar, C.F. Yoder, M.T. Zuber, Mars High Resolution Gravity Fields From MRO, Mars Seasonal Gravity, And Other Dynamical Parameters, Icarus. 211 (2011) 401–428. Https://Doi.Org/10.1016/J.Icarus.2010.10.004.

14. G. Libourel, A.M. Nakamura, P. Beck, S. Potin, C. Ganino, S. Jacomet, R. Ogawa, S. Hasegawa, P. Michel, Hypervelocity Impacts As A Source Of Deceiving Surface Signatures On Iron-rich Asteroids, Sci. Adv. 5 (2019) Eaav3971. Https://Doi.Org/10.1126/Sciadv.Aav3971.

15. S. Marchi, D.D. Durda, C.A. Polanskey, E. Asphaug, W.F. Bottke, L.T. Elkins-tanton, L.A.J. Garvie, S. Ray, S. Chocron, D.A. Williams, Hypervelocity Impact Experiments In Iron-nickel Ingots And Iron Meteorites: Implications For The Nasa Psyche Mission, J. Geophys. Res. Planets. (2020). Https://Onlinelibrary.Wiley.Com/Doi/Abs/10.1029/2019je005927.

16. A. Matter, M. Delbo, B. Carry, S. Ligori, Evidence Of A Metal-rich Surface For The Asteroid (16) Psyche From Interferometric Observations In The Thermal Infrared, Icarus. 226 (2013) 419–427. Https://Doi.Org/10.1016/J.Icarus.2013.06.004.

17. J.M. Mcglaun, S.L. Thompson, M.G. Elrick, Cth: A Three-dimensional Shock Wave Physics Code, International Journal Of Impact Engineering. 10 (1990) 351–360. Https://Doi.Org/10.1016/0734-743x(90)90071-3.

18. H.J. Melosh, E.V. Ryan, E. Asphaug, Dynamic Fragmentation In Impacts: Hydrocode Simulation Of Laboratory Impacts, Journal Of Geophysical Research: Planets. 97 (1992) 14735–14759. Https://Doi.Org/10.1029/92je01632.

19. R. Ogawa, A.M. Nakamura, A.I. Suzuki, S. Hasegawa, Crater Shape As A Possible Record Of The Impact Environment Of Metallic Bodies: Effects Of Temperature, Impact Velocity And Impactor Density, Icarus. 362 (2021) 114410. Https://Doi.Org/10.1016/J.Icarus.2021.114410.

20. M. Ohnaka, A Shear Failure Strength Law Of Rock In The Brittle-plastic Transition Regime, Geophysical Research Letters. 22 (1995) 25–28. Https://Doi.Org/10.1029/94gl02791.

21. E. Pierazzo, A.M. Vickery, H.J. Melosh, A Reevaluation Of Impact Melt Production, Icarus. 127 (1997) 408–423. Https://Doi.Org/10.1006/Icar.1997.5713.

22. S.D. Raducan, T.M. Davison, G.S. Collins, Morphological Diversity Of Impact Craters On Asteroid (16) Psyche: Insight From Numerical Models, J. Geophys. Res. Planets. 125 (2020). Https://Doi.Org/10.1029/2020je006466.

23. F.S. Schwartzberg, Cryogenic Materials Data Handbook, Volume I, Technical Documentary Report, Afml-tdr-64-280, Revised 1970, Air Force Materials Laboratory

24. M.K. Shepard, J. Richardson, P.A. Taylor, L.A. Rodriguez-ford, A. Conrad, I. De Pater, M. Adamkovics, K. De Kleer, J.R. Males, K.M. Morzinski, L.M. Close, M. Kaasalainen, M. Viikinkoski, B. Timerson, V. Reddy, C. Magri, M.C. Nolan, E.S. Howell, L.A.M. Benner, J.D. Giorgini, B.D. Warner, A.W. Harris, Radar Observations And Shape Model Of Asteroid 16 Psyche, Icarus. 281 (2017) 388–403. Https://Doi.Org/10.1016/J.Icarus.2016.08.011.

25. J.H. Tillotson, Metallic Equations Of State For Hypervelocity Impact, General Dynamics San Diego Ca General Atomic Div, 1962.

Https://Apps.Dtic.Mil/Docs/Citations/Ad0486711 (Accessed January 29, 2020).

26. K. Wünnemann, G.S. Collins, H.J. Melosh, A Strain-based Porosity Model For Use In Hydrocode Simulations Of Impacts And Implications For Transient Crater Growth In Porous Targets, Icarus. 180 (2006) 514–527. Https://Doi.Org/10.1016/J.Icarus.2005.10.013.

7 Acknowledgements

We gratefully acknowledge the developers of iSALE-2D Dellen. This work was supported by Southwest Research Institute. A. M. Alexander would like to thank M. Molnar (University of Colorado, National Solar Observatory) for their revision efforts.

8 Data Availability Statement

The experimental crater dimension data used for comparison to simulations in the study are from Marchi et al. (2020). The simulation data generated in this work which are reported in the text in Table 4 and Figures 2 and 3, as well as the compression test data which are reported in Figure 1 will be made available on figshare at https://doi.org/10.6084/m9.figshare.16415907.

We use the iSALE-2D Dellen release of the iSALE shock physics code (Amsden et al., 1980; Collins et al., 2004; Wünnemann et al., 2006). The iSALE-2D Dellen release is distributed on a case-by-case basis to academic users in the impact community, strictly for non-commercial use. Scientists interested in using or developing iSALE may apply to use iSALE at https://isale-code.github.io/access.html.

Version 11.1 of CTH is used for the two impact simulations #2.06 and #2.11. CTH is an Export Controlled software and is available for site license to U.S. Government agencies and contractors working under contract to the U.S. Government or one of its agencies or by a negotiated Limited Commercial License.

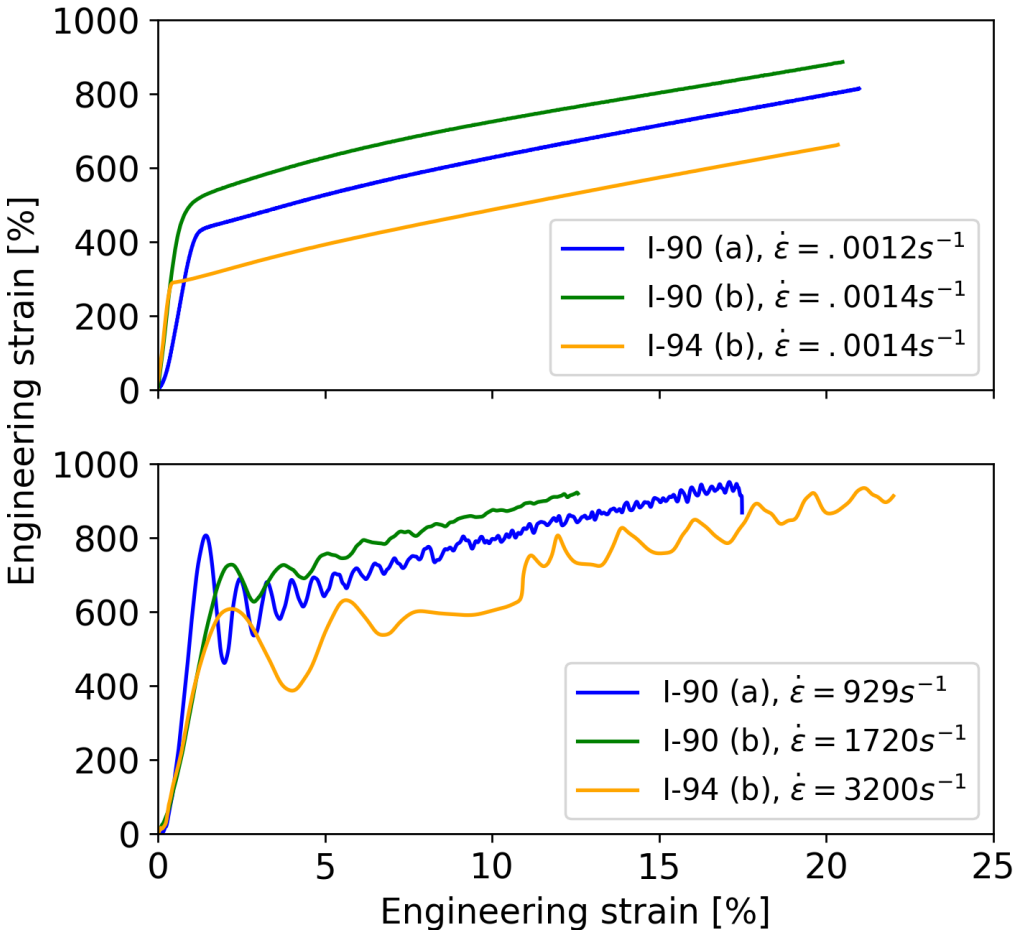

Figure 1. Results from our compression tests on each of the target materials at specified quasistatic strain-rates (top) and high strain-rates (bottom). Multiple tests were performed on each target material (I-90 (a), I-94 (b) and I-90 (b)). Engineering values always use as the reference the initial area or length. Engineering stress is the force divided by the initial area, which is a good estimate of the stress for small changes in area. Engineering strain is the increase in length divided by the initial length.

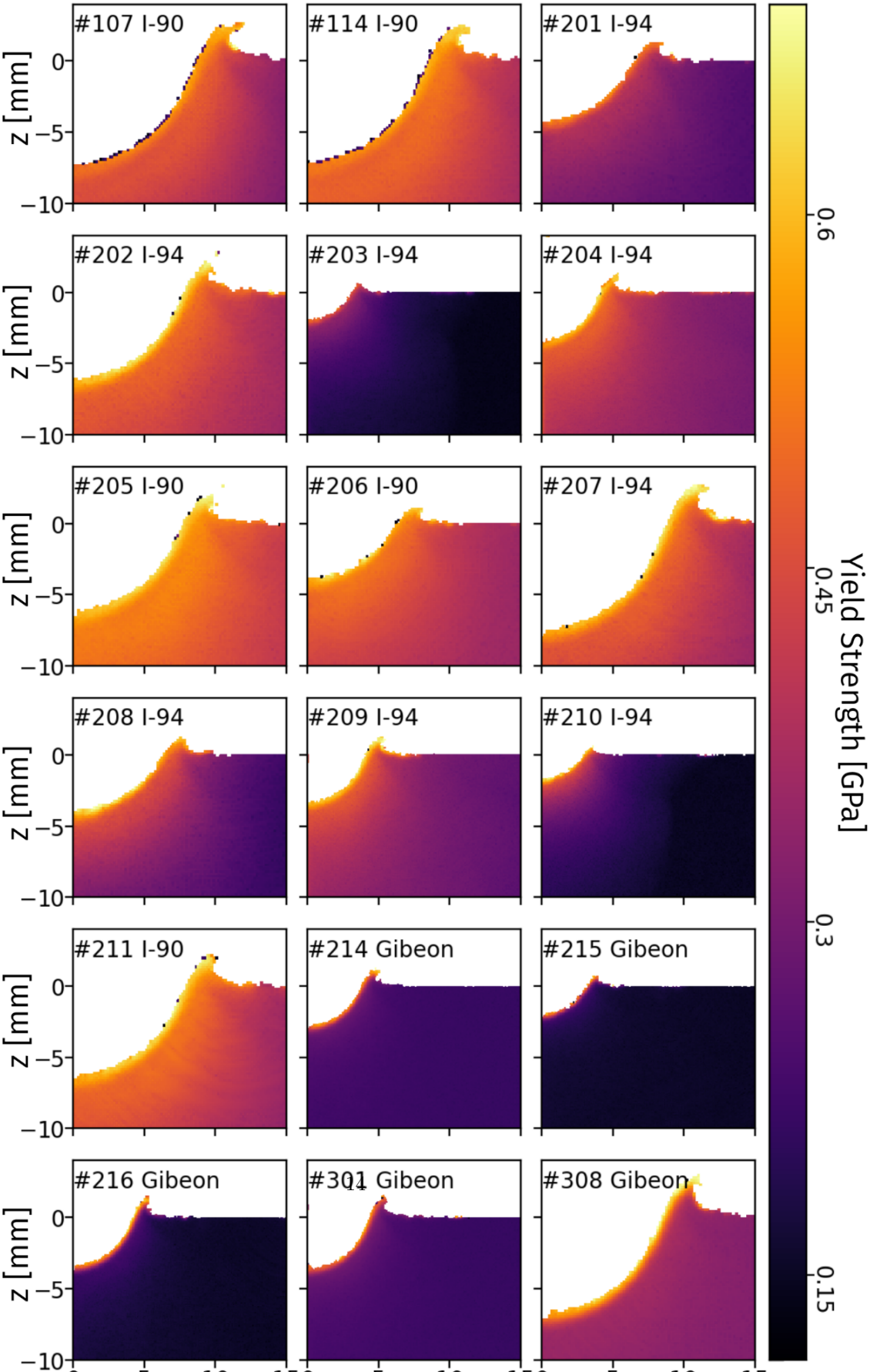
#107 I-90
#114 I-90
#201 I-94
#202 I-94
#203 I-94
#204 I-94
#205 I-90
#206 I-90
#207 I-94
#208 I-94
#209 I-94
#210 I-94
#211 I-90
#214 Gibeon
#215 Gibeon
#216 Gibeon
#301 Gibeon
#308 Gibeon
z [mm]
0
−5
−10
Yield Strength [GPa]
0.6
0.45
0.3
0.15

Figure 2. Simulated crater output from iSALE for simulations into all Fe-Ni ingots from quartz impactors. Each panel is interpreted to be the final crater state at a time step equivalent to 80 microseconds. The crater mesh is colored based on the yield strength for each cell for the given timestep, which ranges from the intact yield stress for the target material (Table 3) down to 1 MPa. There is a mesh mask to exclude cells that have yield stress less than 1 MPa, which are interpreted as numerical artifacts. Crater depth and diameter are measured from the pre-impact surface, or y=0.

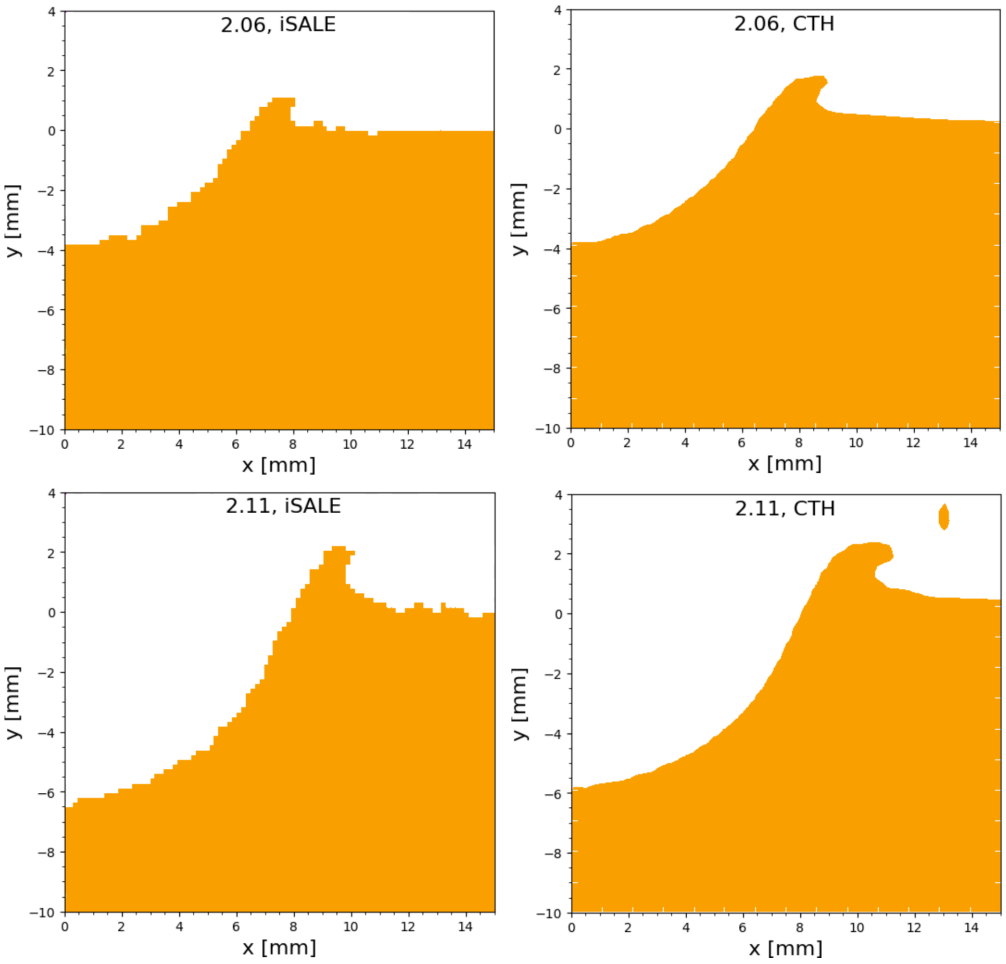

Figure 3. Comparison of iSALE 2D (left) and CTH (right) simulations of experiments #2.06 (top) and #2.11 (bottom). The final geometries of the craters in CTH are 3.7 mm depth and 13.0 mm diameter for #2.06 and 5.9 mm depth and 15.8 mm diameter for #2.11. All dimensions are rounded to the nearest tenth of a millimeter, given that the resolution of the CTH simulations is 0.03 cm.

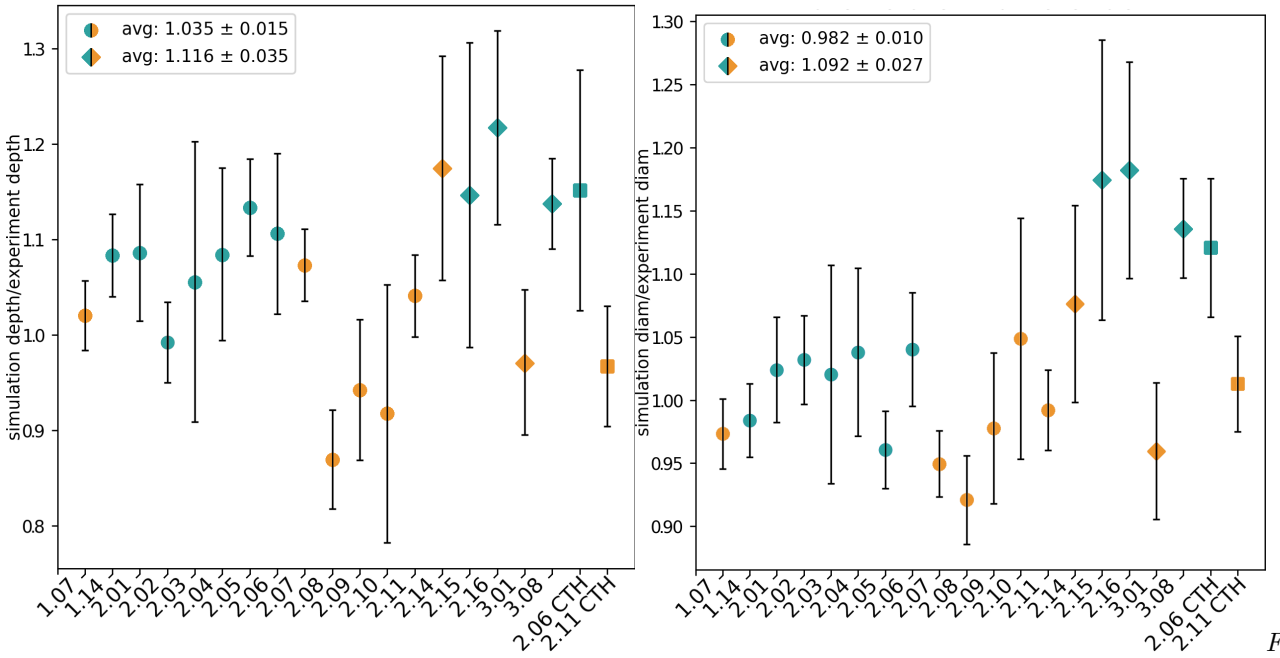

4. Comparing the accuracy of our simulated crater depths (right) and diameters (left) for all simulations. iSALE simulated measurements into ingot materials are denoted as circles, iSALE simulations into Gibeon meteorite targets are denoted as diamonds and the two CTH simulations are shown as squares. Cooled targets are teal and room temperature targets are orange. The mean accuracy for each (iSALE into ingots, iSALE into Gibeon or CTH) are shown in the plot legend. Error bars include the error from measurements of the observed craters and the error attributed to the simulation equivalent to one cell size.

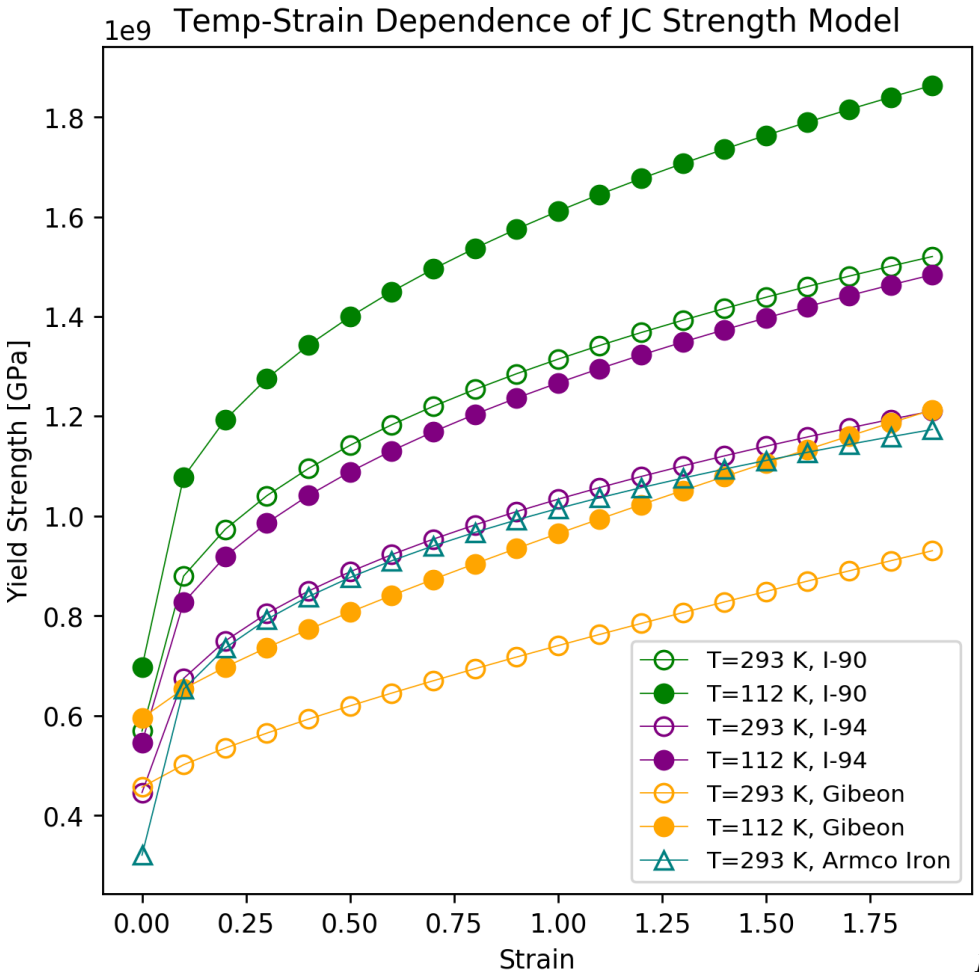

Figure 5. This plot shows the effect temperature has on the yield stress of a material for the JC strength model (Equ. 1). The various colors indicate different target materials from our experiments as well as Armco Iron, which has been used in previous studies as an analog for Psyche (Raducan et al., 2020, Ogawa et al., 2020). Filled points are cooled targets while open points represent room temperature targets. The range of strain reported here = 0-2) is compatible with what is experienced by the target as indicated by our CTH simulations.

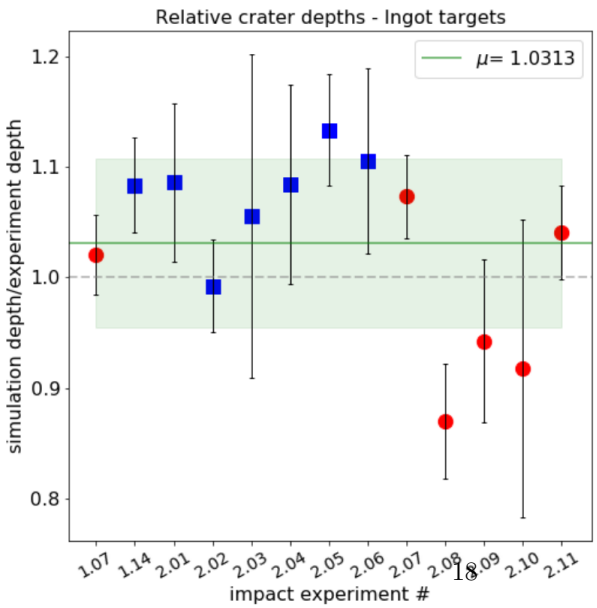
Relative crater depths - Ingot targets
μ= 1.0313
simulation depth/experiment depth
impact experiment #
1.07
1.14
2.01
2.02
2.03
2.04
2.05
2.06
2.07
2.08
2.09
2.10
2.11

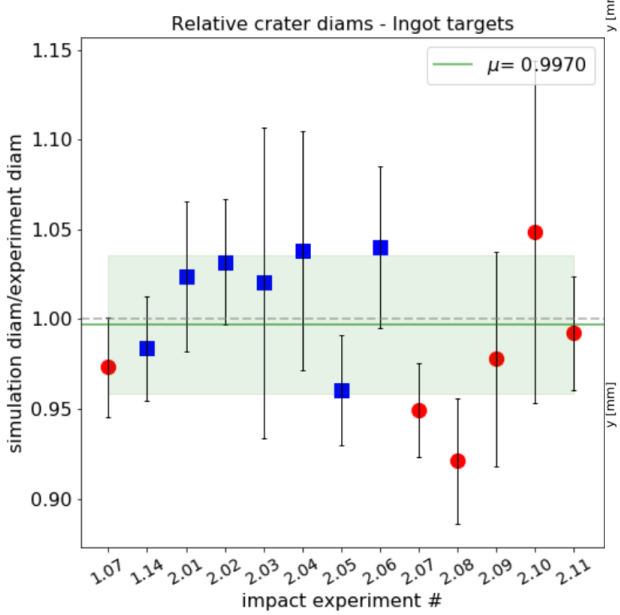
Relative crater diams - Ingot targets
μ= 0.9970
simulation diam/experiment diam
impact experiment #

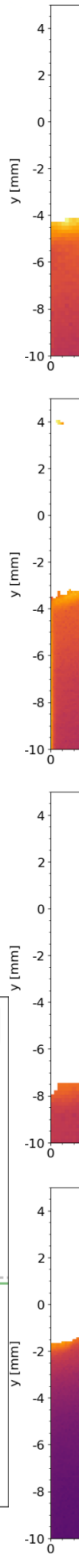
y [mm]